SYNTHESIS, ANTICANCER ACTIVITY, MOLECULAR DOCKING STUDY, OF 4,4-DICHLORO-1,3-OXAZILIDINE-5-ONE DERIVED FROM ISONIAZID

Khalaf A. Jasim[1*], Sheerin Farouq Shaker[1], Dardaa Aziz Ibrahim[1], Zaid A. Dawood[2], Sarab Dalaf Khalaf[3], Adil Hussein Dalaf[1], Andre J. Gesquiere[4, 5]

[1]Department of Chemistry, College of Science, Tikrit University, Tikrit – Iraq.
[2]General directorate of education in governorate of Salah Aldeen, Tikrit, Iraq.
[3]Department of Biology, College of Science, Tikrit University, Tikrit – Iraq
[4]NanoScience Technology Center, University of Central Florida, Orlando, FL 32826, USA.
[5]Department of Chemistry, University of Central Florida, Orlando, FL 32826, USA
[*]e-mail: khalaf.a.jasim@tu.edu.iq

Received 07.01.2025
Accepted 13.05.2025

Abstract: *Breast cancer is considered one of the increasingly serious problems affecting women recently, so many parties are seeking to find effective solutions that reduce its risks. Therefore, the research paper aimed to synthesize hydrazide–hydrazones of isoniazid (T1–T5), which underwent reaction with trichloroacetic acid (TCA), resulting in the synthesis of a series of 4,4-dichloro-1,3-oxazolidine-5-one derivatives (T6–T10) with satisfactory yields. With the use of sophisticated spectroscopic methods such as 13C-NMR, 1H-NMR, and FT-IR, the structure of the recently synthesized compounds was thoroughly verified. The compounds were evaluated for their anticancer potential against the MCF-7 breast cancer cell line. Notably, compounds T7 and T9 exhibited significant anticancer activity, outperforming the reference drug, doxorubicin. A detailed molecular docking study for T7, T9, and doxorubicin was carried out using Autodock Vina software. The binding interactions were assessed by targeting the binding site groove of the human topoisomerase II alpha enzyme (PDB: ID:5GWK). The results revealed favorable RMSD values and strong binding patterns for the compounds, indicating their promising potential as inhibitors.*
Keywords: i*soniazid, 4,4-dichloro-1,3-oxazilidine-5-one, anticancer, molecular docking.*
DOI: 10.65382/2221-8688-2026-2-312-329

1. Introduction

Heterocyclic compounds occupy a high position in organic chemistry and are considered complex and interesting branches of organic chemistry. They greatly contribute to industry and physiological processes [1, 2]. Heterocyclic compounds are pivotal in various fields, such as agriculture, polymers, medicine, etc. These reasons led to diverse work on methods of synthesis and theoretical study [3]. Most drugs contain one or more heterocyclic nuclei [4, 5].

Oxazole is a heterocyclic ring with five members that contains three carbon atoms. The heteroatoms are nitrogen and oxygen [6]. Oxazole has two structural isomers that include 1,3-oxazole and 1,2-isoxazole [7]. Oxazole derivatives have frequently occurred in natural products [7] and synthetic compounds and are recognized as a key skeleton for drug development, such as in Oxaprozin and Azilsartan medoxomil. Many drugs used to treat breast cancer, such as tamoxifen, torimefene, and raloxifene, all these drugs have the same active bioisosters that include tertiary amine [8-11]. As a result of their structural and chemical variety, oxazole-based compounds, as a central scaffold, not only permit numerous forms of interactions with diverse receptors and enzymes, exhibiting extensive biological activities [12, 13], but also play an essential role in medicinal chemistry, demonstrating their immense potential [14, 15]. The fully unsaturated form of oxazole is known as oxazolidine. Occasionally, oxazolidine can be modified by adding functional groups, like a carbonyl group, at different locations (for example, 1,3-Oxazolidine-2-one, 1,3-Oxazolidine-4-one, and 1,3-Oxazolidine-5-one), producing molecules with exceptional biological activity [15, 16]. There have been reports of

numerous oxazoline compounds with anti-cancer properties. *C. Foti et al*., for instance, synthesized a series of oxazolines that contained indole. The substances attach to the colchicine site and prevent tubulin polymerization to produce their anticancer effects [17].

A common bioinformatics modeling technique called "molecular docking" is used to anticipate how a small organic molecule, called a ligand, would bind to its receptor—mostly a protein—and determine its affinity and activity. Hence, molecular docking relates to the rational drug design [18]. Kuntz published the first description of molecular docking in 1982 [19]. A key idea in structure-based virtual screening from its beginning, molecular docking has proved essential to drug discovery. The primary aim of molecular docking research is drug discovery through computer-aided design and evaluation. A variety of programs have been developed, each with its own unique algorithmic foundations [20, 21].

In addition to elucidating biological activities, the molecular docking approach is employed to investigate, model, describe, and analyze the behavior of ligands within the binding site or groove of docked proteins. It examines how a small chemical interacts with the receptor binding site at the atomic level [22]. Molecular docking additionally forecasts the 3D structure of the complexed product, contingent upon the binding characteristics of ligand and target protein overlap [23]. When utilizing a molecular docking tool, the docking process generates numerous potential candidate structures, which are subsequently ranked and organized based on a scoring system [23-25].

In this paper, we tried to design new oxazoline derivatives and investigate their activity as candidate compounds against breast cancer with a molecular modeling study against a cancer receptor called the human topoisomerase II alpha enzyme (PDB: ID: 5GWK). Where some synthesized compounds showed good anticancer activity with the best docking results.

2. Experimental part

2.1. Equipment and Chemicals. The solvents and reagents used in this study were purchased from Fluka and BDH and were employed exactly as specified. Thin layer chromatography (TLC) on silica gel GF254 (type 60) pre-coated aluminum sheets were used to monitor the reaction's progress, with iodine vapor employed to visualize the spots. The melting point was determined using an open glass capillary method on a Stuart SMP40. The Fourier-transform infrared spectroscopy (FT-IR, SHIMADZU 600), ^{1}H-NMR, and ^{13}C-NMR were used to get the spectral data.

Table 1. Some physical characteristics of starting compounds

Comp. No.	M.F.	M.Wt	M.P. ^{o}C	Color
Izoniazide	$C_6H_7N_3O$	137	171.4	Dark yellow
benzaldehyde	C_7H_6O	106	-57	Colorless
p-chlorobenzaldehyde	$C_{13}H_{10}N_4O_3$	140.57	47	white
p-nitro benzaldehyde	$C_{14}H_{13}N_3O_2$	255.28	103-106	Yellow
p-N, N dimethyl amino benzaldehyde	$C_9H_{11}NO$	149	72-75	white
p-methoxy benzaldehyde	$C_{15}H_{11}N_3O_3$	136	0.00	Brown

2.2. Preparation of isonicotinic hydrazide - hydrazone derivatives (T1-T5) [25]. 0.01 mol of para-derivatives of benzaldehyde was dissolved in 50 mL of absolute ethanol (EtOH. Abs) in a 250 mL round-bottom flask with two necks. The mixture was heated and stirred for five minutes to ensure complete dissolution. Then, 0.01 mol of isonicotinohydrazide (amine), previously dissolved in 25 mL of ethanol in a separate

container, was added drop by drop through a distillation funnel. The mixture was refluxed for three to six hours. As the reaction progressed, a precipitate formed, and thin layer chromatography (TLC) using a solvent mixture of diethyl ether and benzene (9:1) was employed to monitor the reaction. After cooling, the reaction mixture was filtered using a Büchner funnel and recrystallized using an appropriate solvent mixture.

2.3. Preparation of 4,4-dichloro-1,3-oxazolidinone-5-one derivatives (T6-T10) [26]. 0.02 moles of the **(T1-T5)** derivatives were dissolved in 25 mL of 1,4-dioxane in a 100 mL round-bottom flask, mixed, and heated in a water bath for ten minutes. In a separate container, 25 mL of 1,4-dioxane was combined with 0.2 mg of trichloroacetic acid (TCA), and five drops of triethylamine (Et_3N) were added to the first solution. The TCA solution was then added dropwise to the hydrazide-hydrazine derivative solution while stirring. The reaction mixture was refluxed for ten hours. Upon completion, the formation of a precipitate was observed, which was then filtered and recrystallized from chloroform. The progress of the reaction was monitored by thin-layer chromatography (TLC) using a benzene:methanol solvent mixture (6:4).

2.4. Molecular docking [27]. Molecular docking studies were conducted using AutoDock Vina software. The human topoisomerase IIalpha enzyme (PDB ID: **5GWK**) was obtained from the RCSB Protein Data Bank (PDB) website. The MM2 method in Chem3D software was employed to minimize the energy of the new derivatives. For enzyme preparation, polar hydrogens were added, and water molecules were removed. The ligand and protein were prepared using AutoDockTools 1.5.6 software. Finally, the 2D and 3D binding modes were visualized using Discovery Studio 2020 Client [29].

2.5. MTT Assay Protocol. A: In this step, 1×10^4 cells were seeded into each well of a 96-well microplate. The plate was then incubated at 37°C for 24 hours until 60% confluence was achieved.

B: On the second day, doxorubicin and oxazoline derivatives were administered to the cells in sterile microtubes at various concentrations (15.625, 31.25, 62.5, 125, 250, and 500 µg/mL).

C: On the third day, the top medium was removed from the wells, and 100 µL of MTT dye (0.5 mg/mL) was added to each well. The plates were then incubated in the dark for 24 hours. After removing the top medium, 100 µL of DMSO was added to each well. The plates were shaken for 20 minutes in the dark to dissolve the formazan crystals. Finally, the intensity of the resulting color was measured at 570 nm using a microplate reader (DNM-9602G).

3. Results and Discussion

3.1. Identification of Synthetic Derivatives. Hydrazide-hydrazone derivatives **(T1-T10)** were synthesized by reacting para-derivatives of benzaldehyde with isonicotinohydrazide in dioxane.

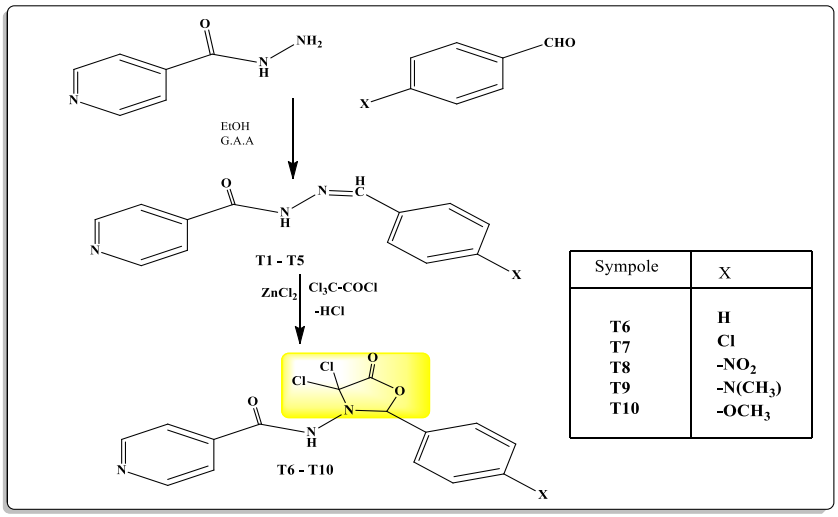

Scheme 1. Synthesis of Oxazoline Compounds (T6-T10)

Subsequently, as depicted in Scheme 1, the hydrazide-hydrazone derivatives (D1-D5) were treated with trichloroacetic acid to produce 1,3-thiazinan-4-one derivatives (A6-A10). The identities of these derivatives were confirmed through spectral analysis. The physical properties of the synthetic derivatives are summarized in Table 2.

Table 2. Some physical characteristics of (T1-T10) compounds

Comp. No.	M.F.	M.Wt.	X	M.P. °C	R_f	Time hr.	Color	Yield%
T1	$C_{13}H_{11}N_3O$	225.25	H	193-195	0.46	3	Dark yellow	74
T2	$C_{13}H_{10}N_3OCl$	259.69	Cl	140-142	0.73	6	Yellow	80
T3	$C_{13}H_{10}N_4O_3$	270.25	NO_2	159-161	0.80	4	Brown	81
T4	$C_{14}H_{13}N_3O_2$	255.28	OCH_3	175-176	0.76	4	White	73
T5	$C_{15}H_{16}N_4O$	268.32	$N(CH_3)_2$	136-137	0.55	5	Orange	70
T6	$C_{15}H_{11}N_3O_3$	281.33	H	204-206	0.77	12	Brown	64
T7	$C_{15}H_{10}N_3O_3Cl$	316.82	Cl	223-225	0.49	10	Dark brown	73
T8	$C_{15}H_{10}N_4O_5$	327.37	NO_2	211-213	0.82	9	Light orange	70
T9	$C_{17}H_{15}N_4O_3$	324.32	$N(CH_3)_2$	231-233	0.52	12	Off white	56
T10	$C_{16}H_{12}N_3O_4$	312.2	OCH_3	193-195	0.40	10	Brown	79

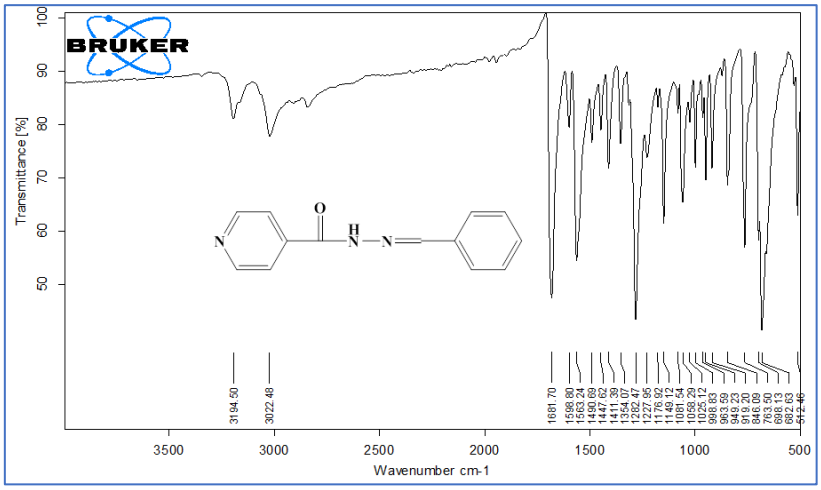

Fig. 1. FT-IR picture of T1 derivative

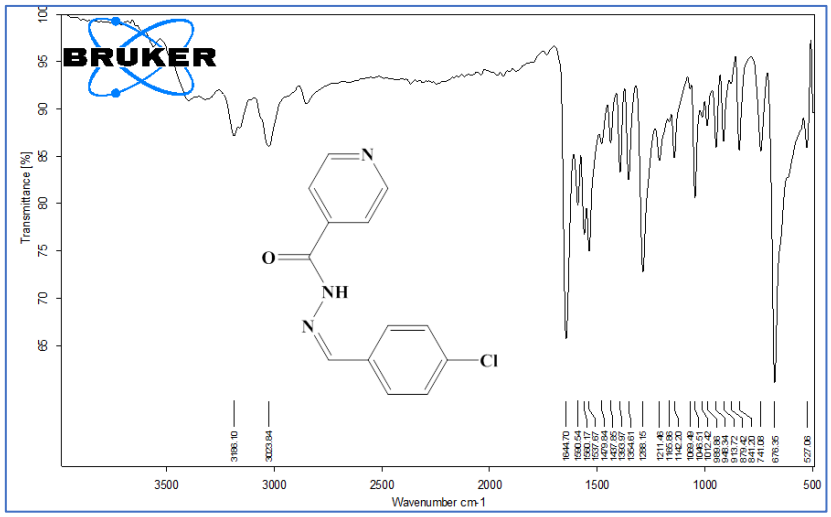

Fig. 2. FT-IR picture of T2 derivative

This reaction happened through a nucleophillic attack cyclization mechanism to afford a five-membered ring.

3.1.1. Compound Identification by FT-IR. Spectral techniques were employed to confirm the proposed structures of the synthesized compounds. As shown in Fig.s 1–5, the FT-IR spectra of T1–T5 exhibit a vibration

frequency peak for the azomethine C=N group within the range of 1638–1659 cm^{-1}, along with bands at 3137–3204 cm^{-1} corresponding to N-H stretching. Additional bands at 3022–3041 cm^{-1} are attributed to C–H aromatic stretching, while peaks in the range of 1644–1684 cm^{-1} correspond to the C=O group. A peak at 1475–1497 cm^{-1} is assigned to the C=C aromatic stretch, and a band at 1229–1282 cm^{-1} indicates C–N stretching.

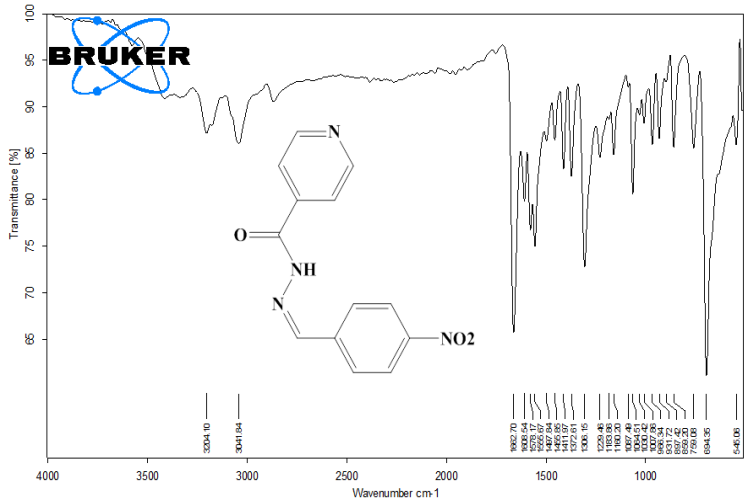

Fig. 3. FT-IR picture of T3 derivative

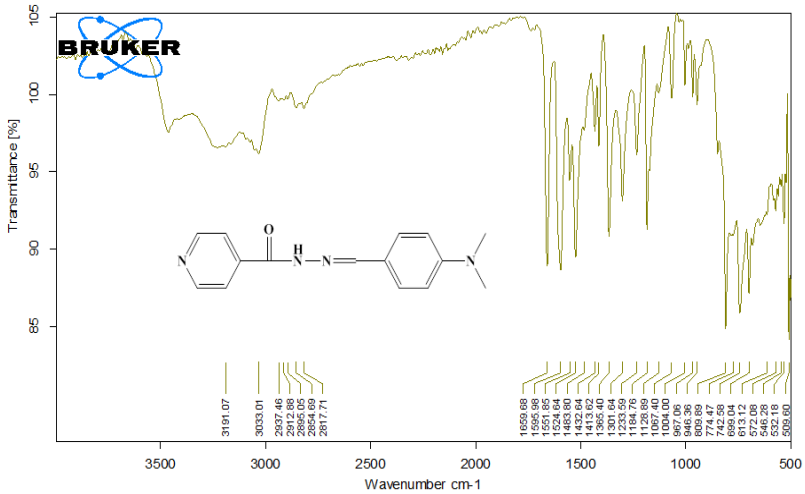

Fig. 4. FT-IR picture of T4 derivative

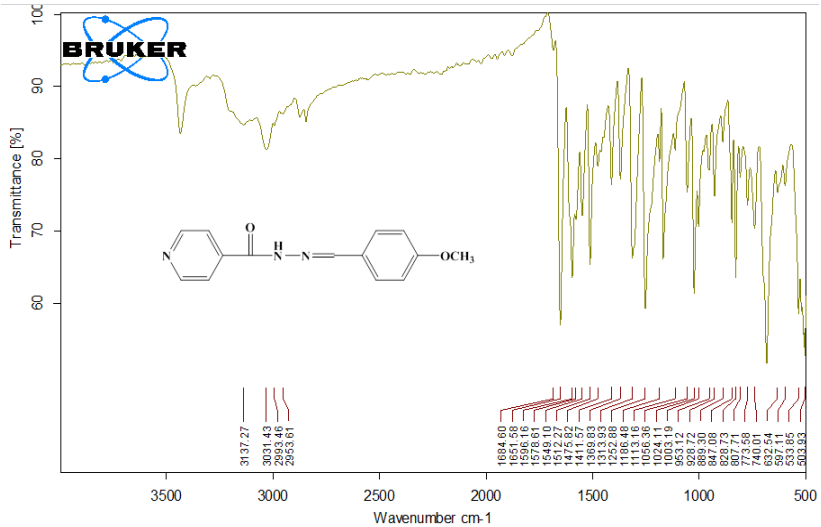

Fig. 5. FT-IR picture of T5 derivative

For the 1,3-oxazolidine-5-one derivatives T6–T10, the FT-IR spectra reveal the following results: Strong, distinct peaks in the range of 1683–1754 cm^{-1} correspond to the C=O group within the oxazolidine ring, while the azomethine HC=N peaks in the range of 1638–1659 cm^{-1} are no longer observed. The peaks at 3034–3093 cm^{-1} are attributed to C-H aromatic stretching, and bands in the 2860–2980 cm^{-1} region suggest the presence of C–H aliphatic groups. The C=O group from the isoniazid moiety is represented by peaks between 1646 and 1668 cm^{-1}, while C=C aromatic stretching is reflected in bands at 1566–1610 cm^{-1} and 1427–1507 cm^{-1}. Additionally, as shown in Fig.s 6–10, bands in the 1230–1298 cm^{-1} range are indicative of C–N bond stretching.

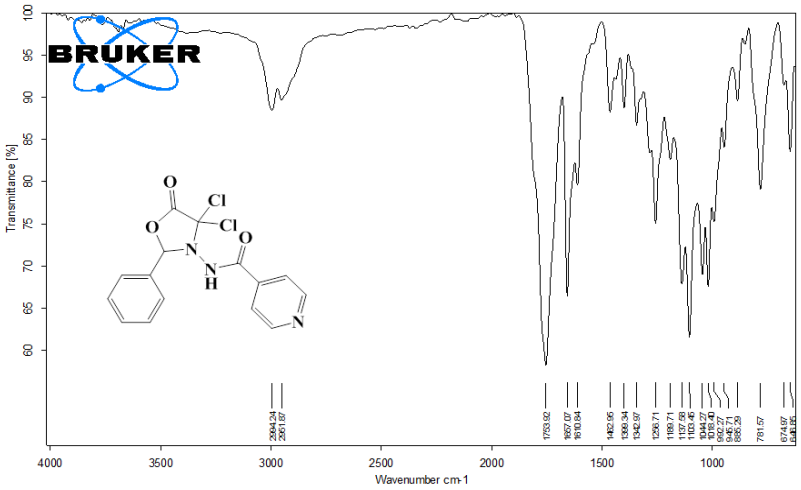

Fig. 6. FT-IR picture of T6 derivative

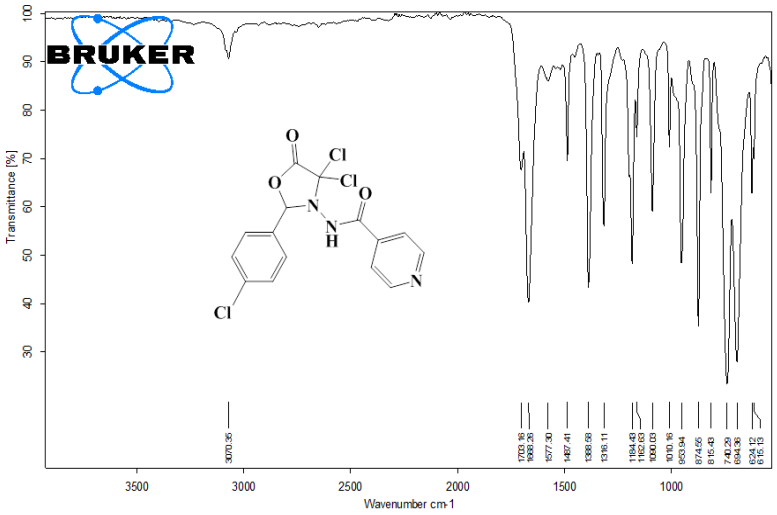

Fig. 7. FT-IR picture of T7 derivative

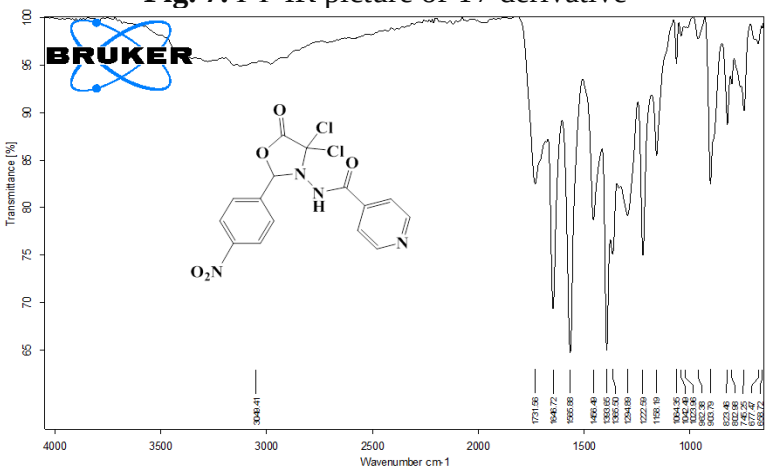

Fig. 8. FT-IR picture of T8 derivative

The proton nuclear magnetic resonance (^{1}H-NMR) spectra of the 1,3-oxazolidine-5-one derivatives T6–T10 were interpreted as follows: For T6, the NH proton is represented by a singlet signal at δ = 9.85 ppm (1H), while the aromatic protons of the benzene and pyridine rings produce a multiplet signal in the range of δ = 7.22–8.67 ppm. The HDO proton appears as a doublet signal at δ = 3.36 ppm. A signal in the range of δ = 2.49–2.51 ppm is observed, which is indicative of DMSO-d6, the deuterated solvent [30].

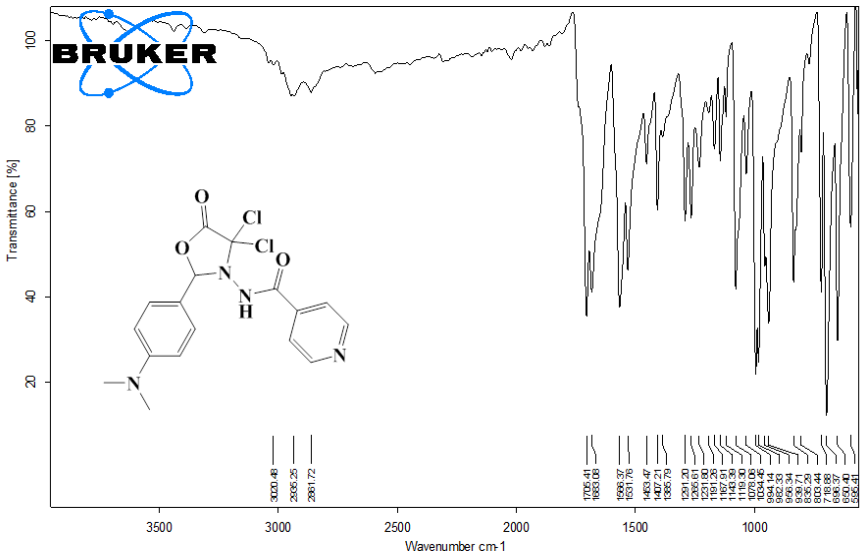

Fig. 9. FT-IR picture of T9 derivative

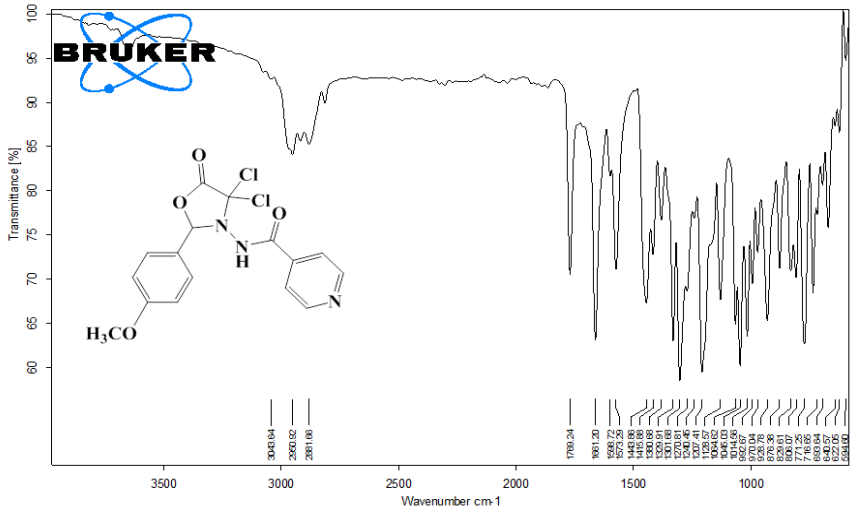

Fig. 10. FT-IR picture of T10 derivative

3.1.2. Compound Identification Using ^{1}H-NMR Spectroscopy. The ^{1}H-NMR spectrum of compound **T7**, as depicted in Fig. 11, displayed a signal in the range of δ = 2.49 - 2.51 ppm corresponding to exchangeable protons from the deuterated solvent DMSO-d6. A singlet at δ = 9.69 ppm (1H) was observed, which corresponds to the NH proton. Additionally, a multiplet in the range of δ = 7.29 - 8.70 ppm was seen, representing the aromatic protons from the benzene and pyridine rings.

These signals provide essential information for confirming the structural features of T7, including the identification of functional groups such as the NH group (likely from an amine or amide) and the aromatic protons associated with the benzene and pyridine rings [31].

The ^{1}H-NMR spectrum of compound **T8**, presented in Fig. 12, shows a splitting signal at δ = 9.90 ppm (1H), which is attributed to the NH proton. Multiple splitting signals between δ = 7.32 and 8.75 ppm are observed, corresponding to the aromatic protons in the benzene and

pyridine rings. A splitting signal at δ = 3.38 ppm is assigned to the exchangeable HDO proton, while the signal between δ = 2.51 and 2.53 ppm corresponds to the exchangeable protons from the deuterated solvent DMSO-d^6.

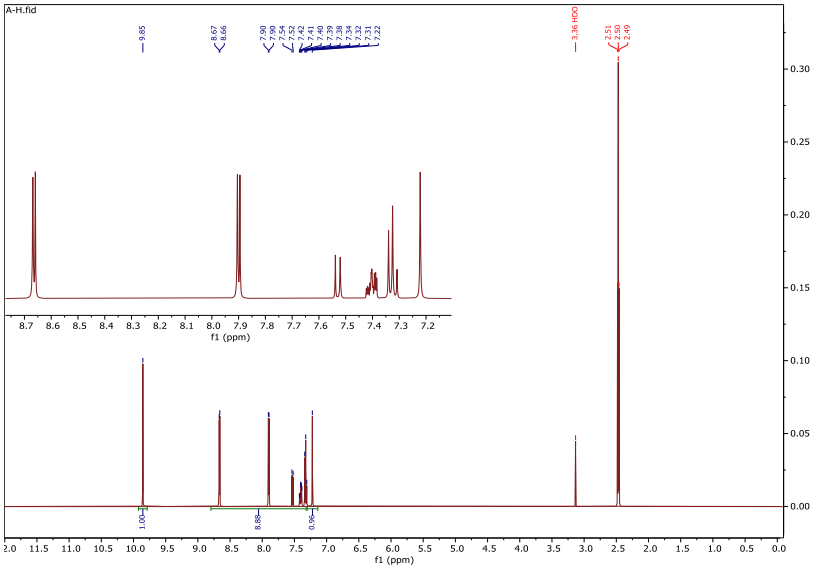

Fig. 11. ^{1}H-NMR picture of T**7** derivative

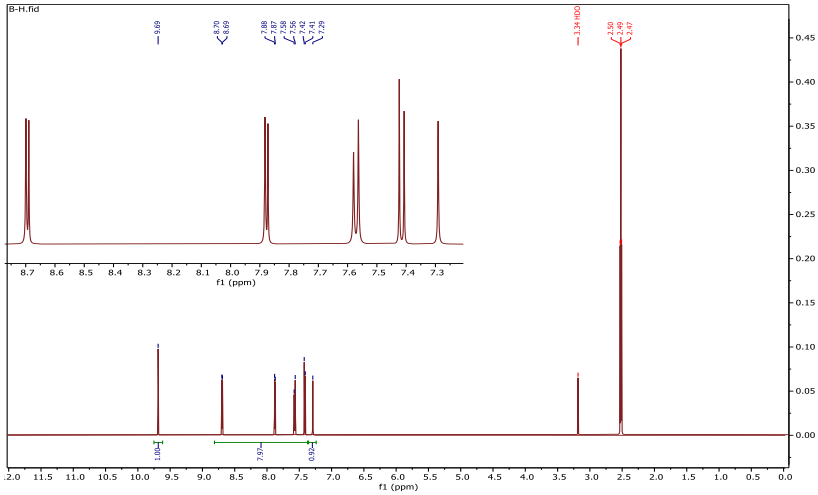

Fig. 12. ^{1}H-NMR picture of T8 derivative

This spectrum provides crucial structural information for T8, identifying the exchangeable protons (from HDO and DMSO-d^6), the NH proton, and the aromatic protons of the benzene and pyridine rings [28].

The ^{1}H-NMR spectrum of compound **T9**, presented in Fig. 13, reveals a singlet at δ = 9.79 ppm (1H), corresponding to the NH proton. The aromatic protons of the benzene and pyridine rings are represented by multiple splitting signals within the range of δ = 6.84 - 8.83 ppm. Two methyl groups (-N(CH$_3$)$_2$) are identified by a singlet at δ = 2.98 ppm, with an integral value of six protons. The HDO exchangeable proton is observed as a singlet at δ = 3.38 ppm, while the exchangeable protons from the deuterated solvent (DMSO-d^6) are represented by a signal at δ = 2.46 - 2.48 ppm. This analysis provides key structural insights into compound T9, including the identification of the NH proton, aromatic protons, methyl groups, HDO exchangeable protons, and solvent-related exchangeable protons [30].

The ^{1}H-NMR spectrum of compound **T10**, shown in Fig. 14, reveals several splitting signals in the range of δ = 6.96 - 8.66 ppm, which are attributed to the aromatic protons in the benzene and pyridine rings. A singlet signal at δ = 3.92 ppm, with an integral value corresponding to three protons, is assigned to two methyl groups (-OCH$_3$). A singlet signal at δ = 3.36 ppm is attributed to the exchangeable HDO proton,

while the exchangeable protons from the deuterated solvent (DMSO-d^6) are represented by a signal at δ = 2.49 - 2.52 ppm. This data provides important structural information for T10, including the identification of aromatic protons, methoxy groups, HDO exchangeable protons, and solvent-related exchangeable protons [32-37].

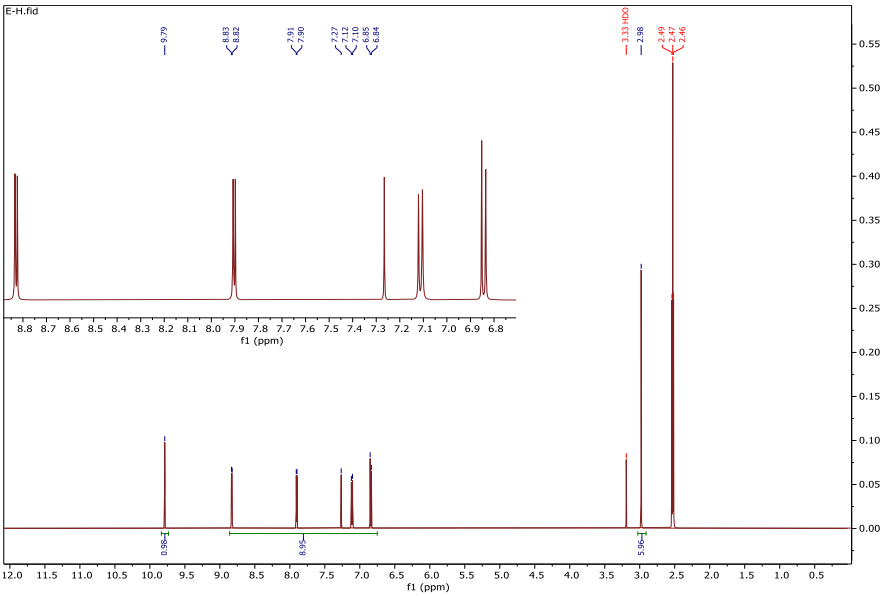

Fig. 13. ^{1}H-NMR picture of T9 derivative

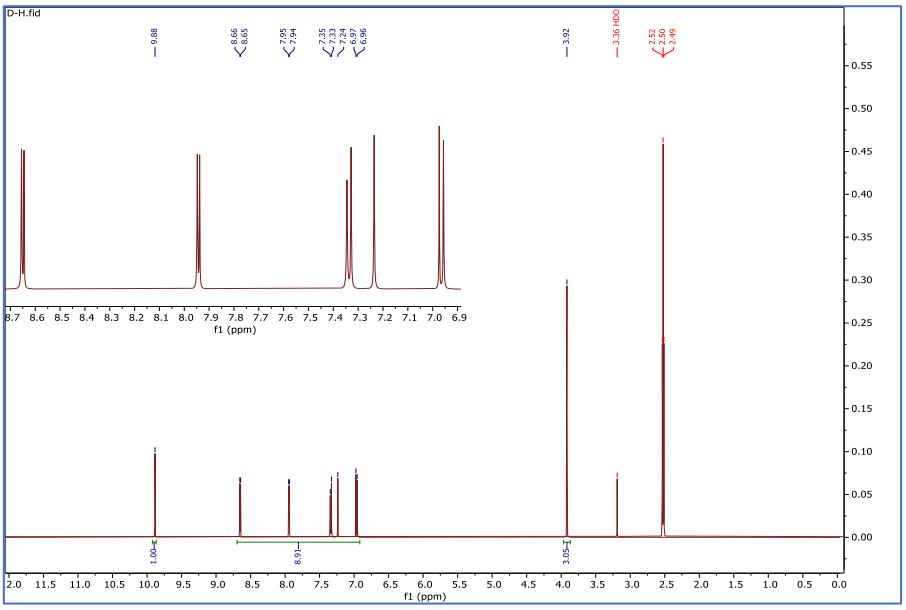

Fig. 14. ^{1}H-NMR picture of T10 derivative

3.1.3. Compound Identification Using ^{13}C-NMR. The ^{13}C-NMR spectrum for compound **T6** reveals a signal at δ = 93.86 ppm, corresponding to the carbon atom at the 2-position in the oxazolidine ring. A signal at δ = 119.8 ppm is assigned to the carbon at the 4-position (CCl_2). The signals in the range of δ = 122 - 155.57 ppm are attributed to the aromatic carbons in the benzene and pyridine rings. A signal at δ = 163.69 ppm corresponds to the C=O group of the isonicotinic moiety, while a signal at δ = 166.7 ppm is assigned to the C=O group at the 5-position in the oxazolidine ring. Additionally, a signal at δ = 39.29 - 40.55 ppm corresponds to DMSO. This ^{13}C-NMR data provides valuable structural information for compound T6, including the identification of carbon atoms in the oxazolidine ring, aromatic carbons, and carbonyl groups, as well as DMSO-related signals.

The ^{13}C-NMR spectrum of compound **T7**, shown in Fig. 15, reveals a signal at δ = 93.86

ppm, corresponding to the carbon atom at the 2-position of the oxazolidine ring. The aromatic carbons of the pyridine and benzene rings are represented by signals in the δ = 120–150 ppm range. A signal at δ = 168 ppm is attributed to the C=O group at the 5-position in the oxazolidine ring, while a signal at δ = 165 ppm corresponds to the C=O group in the isonicotinic moiety. Signals in the δ = 40 ppm region are assigned to the carbons of DMSO-d^6.

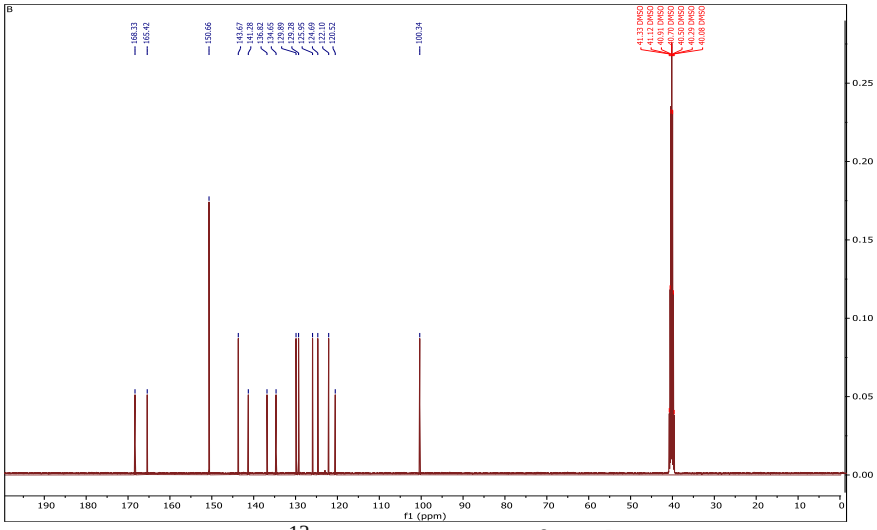

Fig. 15. ^{13}C-NMR picture of T7 derivative

The ^{13}C-NMR spectrum of compound **T8**, as shown in Fig. 16, reveals a signal at δ = 100 ppm, corresponding to the carbon atom at the 2-position of the oxazolidine ring. Signals in the δ = 120–150 ppm range are attributed to the aromatic carbons of the pyridine and benzene rings. The C=O group of the isonicotinic moiety produces a signal at δ = 161.82 ppm, while the C=O group at the 5-position in the oxazolidine ring is responsible for a signal at δ = 168 ppm. Signals around δ = 40 ppm are assigned to the carbons of DMSO-d^6.

The ^{13}C-NMR spectrum of compound **T9** reveals a signal at δ = 44.40 ppm, corresponding to the two carbon atoms of the -N(CH_3)$_2$ group. The carbon atom at the 2-position of the oxazolidine ring is represented by a signal at δ = 103 ppm, while the carbon atom at the 4-position (CCl_2) in the oxazolidine moiety produces a signal at δ = 114 ppm. Signals in the δ = 125–149 ppm range are attributed to the aromatic carbons of the pyridine and benzene rings. Additionally, signals at δ = 154 and 157 ppm are likely associated with the C=N carbon of the pyridine ring. The C=O group in the isonicotinic moiety produces a signal at δ = 161 ppm, while the C=O group at the 5-position in the oxazolidine ring generates a peak at δ = 170 ppm. The carbons from DMSO-d^6 are responsible for the signals observed around δ = 40 ppm.

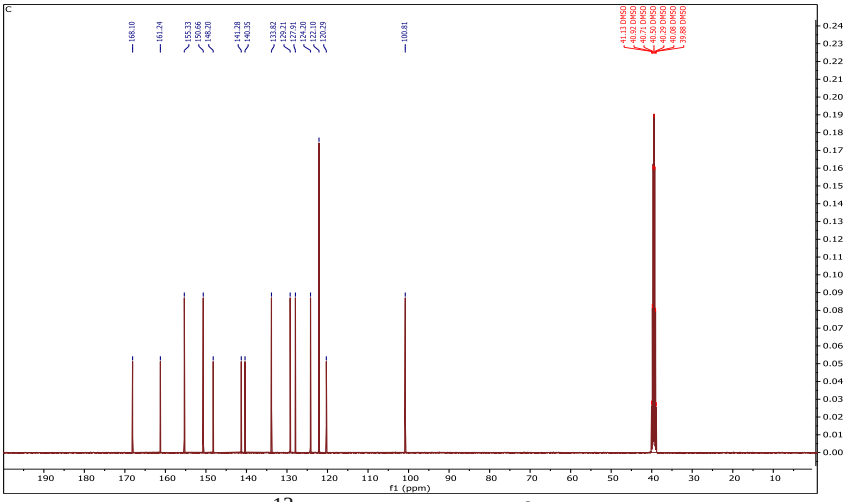

Fig. 16. ^{13}C-NMR picture of T8 derivative

The ^{13}C-NMR spectrum of compound **T10**, shown in Fig. 17, reveals a signal at δ = 60.63 ppm, which corresponds to the carbon atoms of the methoxy group (-OCH_3) attached at the para position on the benzene ring. The carbon atom at the 2-position of the oxazolidine ring is represented by a signal at δ = 94.35 ppm, while the carbon atom at the 4-position (CCl_2) in the oxazolidine moiety generates a signal at δ = 112 ppm. The aromatic carbons in the pyridine and benzene rings are represented by signals in the δ = 114–150 ppm range. The C=N carbon in the pyridine ring is likely responsible for the signals at δ = 154 and 159 ppm. The C=O group in the isonicotinic moiety generates a peak at δ = 165 ppm, while the C=O group at the 5-position in the oxazolidine ring produces a peak at δ = 168 ppm. The carbons from DMSO-d^6 are responsible for the signals observed at δ = 40 ppm.

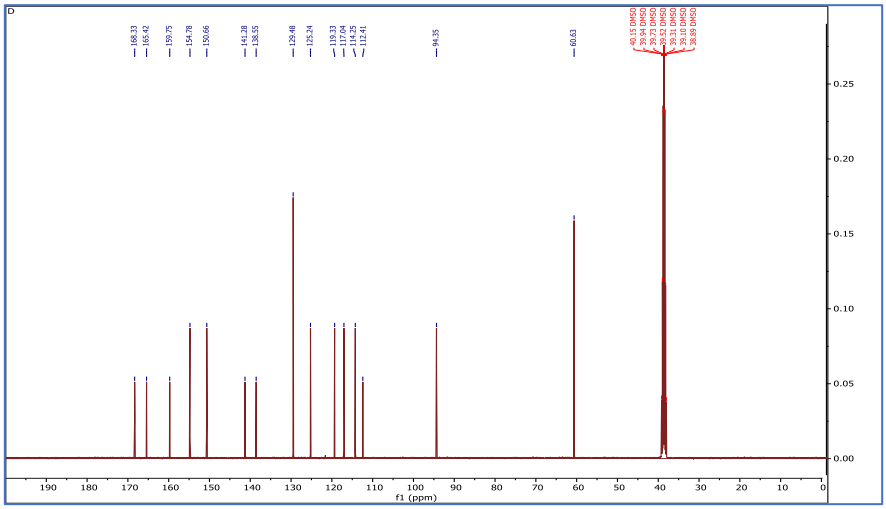

Fig. 17. ^{13}C-NMR picture of T10 derivative

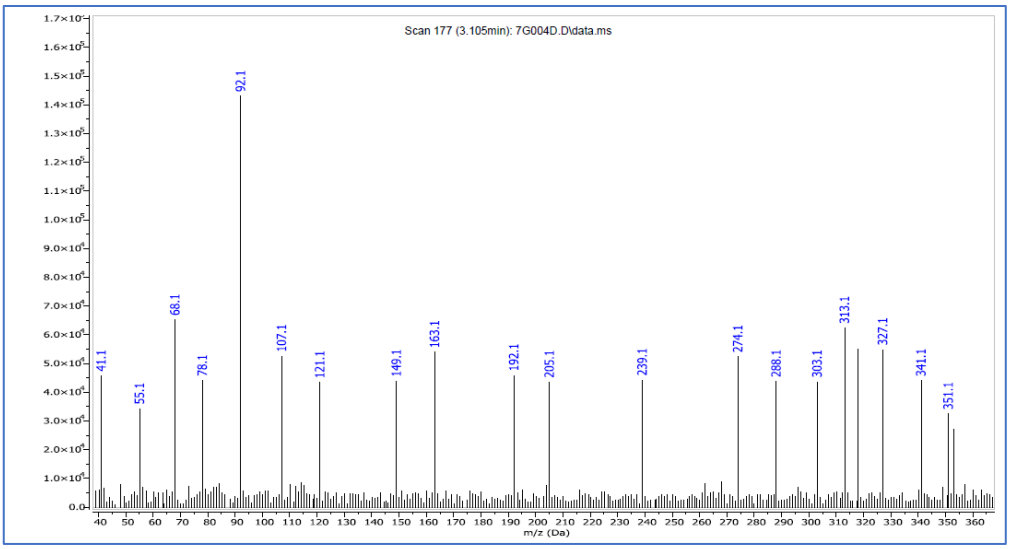

Fig. 18. Mass spectrum picture of T6 derivative

3.1.4. Compound Identification Using Mass Spectrometry. Mass spectrometry was employed to characterize the oxazolidinone derivatives T6-T10. The results indicated that the calculated and recorded molar masses agreed. For compound **T6**, shown in Figure 18, the molecular weight was found to be 351.1 g/mol, with the base peak corresponding to the acylium ion at 93.1 g/mol.

In the mass spectrum of compound **T7** (Fig. 19), the molecular weight was observed at 384 g/mol, with the base peak at 93.1 g/mol corresponding to the acylium ion. For compound **T8** (Fig. 20), the molecular weight was found to be 396 g/mol, with the base peak at 92.1 g/mol, representing the acylium ion.

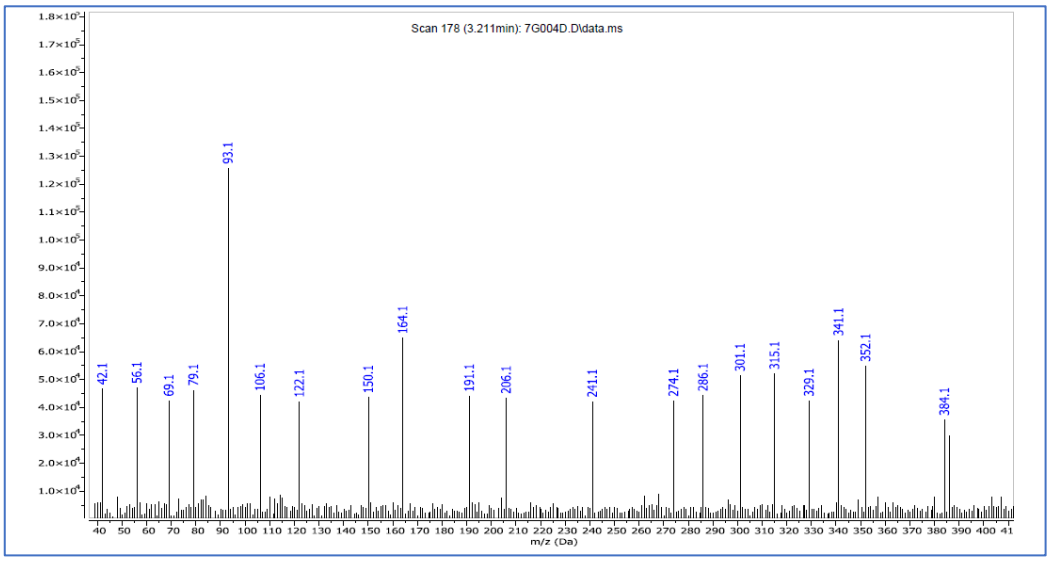

Fig. 19. Mass spectrum picture of T7 derivative

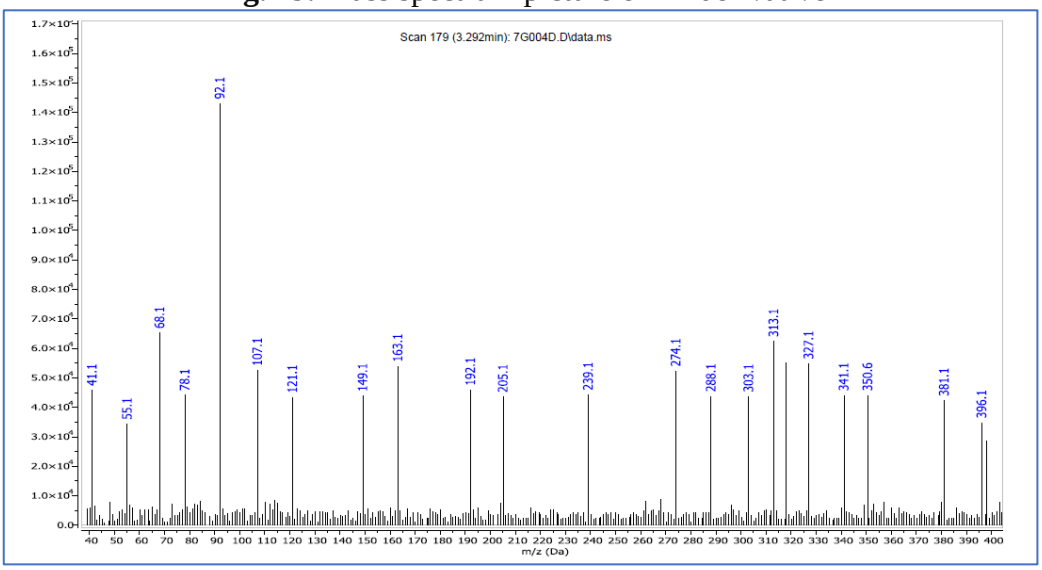

Fig. 20. Mass spectrum picture of T8 derivative

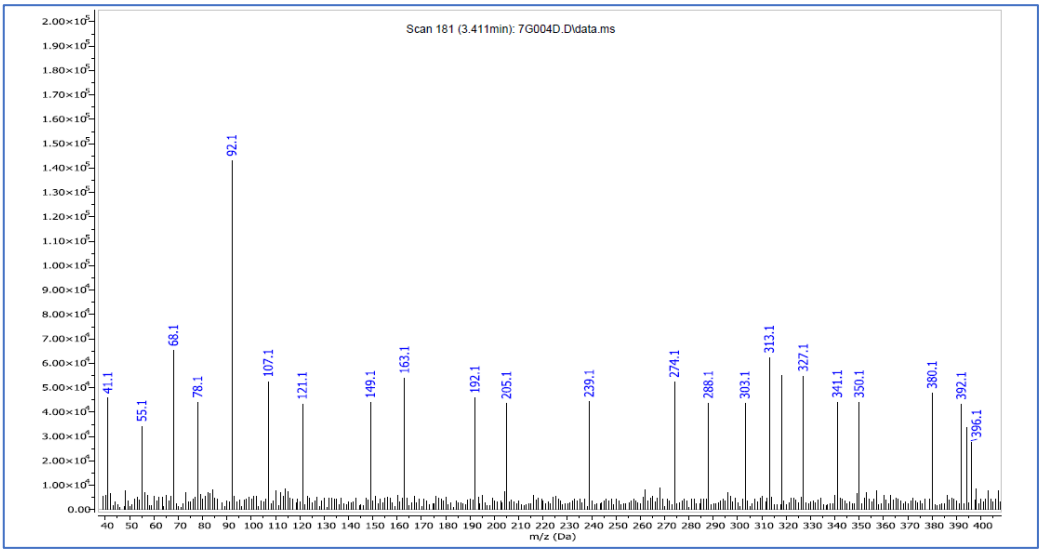

Fig. 21. Mass spectrum picture of T9 derivative

The mass spectrum of compound **T9** (Fig. 21) showed a peak at 396.1 g/mol, indicating the molecular weight, and a base peak at 92.1 g/mol, corresponding to the acylium ion. Similarly, the

mass spectrum of compound **T10** (Fig. 22) displayed a peak at 381 g/mol, representing the molecular weight, and a base peak at 93.1 g/mol, associated with the acylium ion.

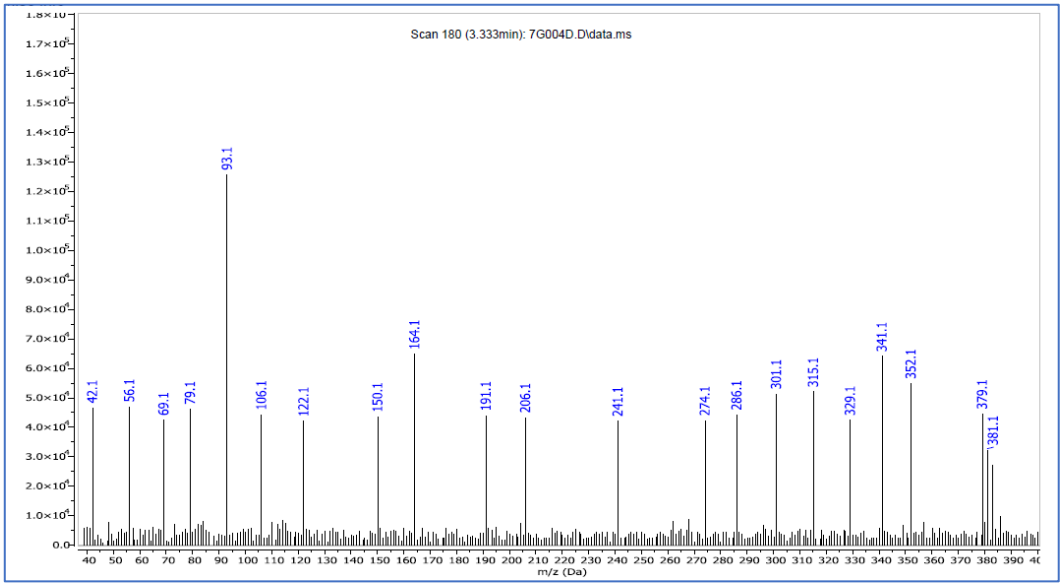

Fig. 22. Mass spectrum picture of T10 derivative

3.2. Molecular Docking Analysis of Derivatives T6–T10 of 4,4-Dichloro-1,3-Oxazolidine-5-One. To evaluate the inhibitory effects of compounds **T7, T9**, and **doxorubicin**, a molecular docking simulation was conducted against the binding site of human topoisomerase **II alpha**. The results indicated that compound **T7** interacted with the binding site, exhibiting a binding free energy of -8.1 **kcal/mol**. This interaction was mediated through one hydrogen bond, as well as pi-anion and pi-pi stacking interactions with the amino acid residues, as shown in Fig. 23.

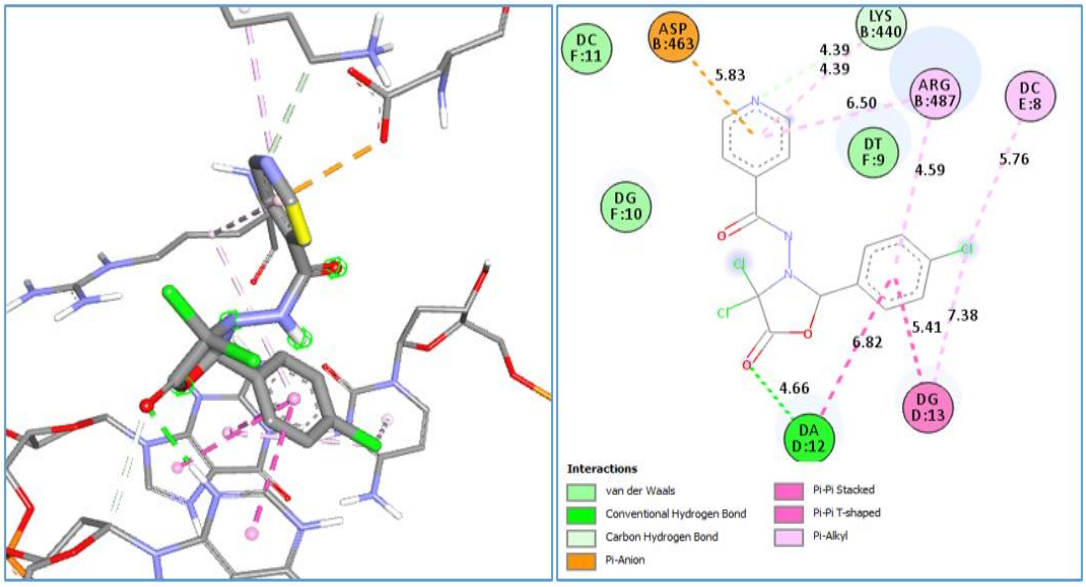

Fig. 23. The interaction between compound T7 with Human topoisomerase IIalpha enzyme(PDB:ID:5GWK) in 3D and 2D dimensions

The root mean square deviation (RMSD) value for this interaction was 0.035 Å. With a binding free energy of -8.2 kcal/mol, compound T9 interacts with the amino acid residues of the binding site through hydrogen bonds with SER: A:802, involving the C=O group of the dichloro oxazoline moiety, and DT: D:9, with the NH group, among other interactions. As shown in

Fig. 24, pi-alkyl interactions were observed in this simulation, with an RMSD value of 0.052 Å. In the case of doxorubicin, it interacts with the binding site through three hydrogen bonds: ASP: B:463 with OH and OCH3, and ARG: B:487 with the O atom in the hydroplane ring. Additionally, Pi-alkyl, amide-Pi stacking, and Pi-Pi T-shaped interactions contribute to the binding mode, resulting in a binding free energy of -10.5 kcal/mol. The RMSD value for doxorubicin's binding is 2.354 Å, as seen in Fig. 25. The binding free energy and RMSD values for these compounds are summarized in Table 3.

Table 3. The values of the binding energies between the prepared compounds (T6-T10) with binding site of Human topoisomerase IIalpha enzyme (PDB: ID:5GWK)

Comp. No.	T7	T9	doxorubicin
RMSD(A°)	3.144	3.55	2.354
Docking Score(kcal/mol)	-8.1	-8.2	-10.5

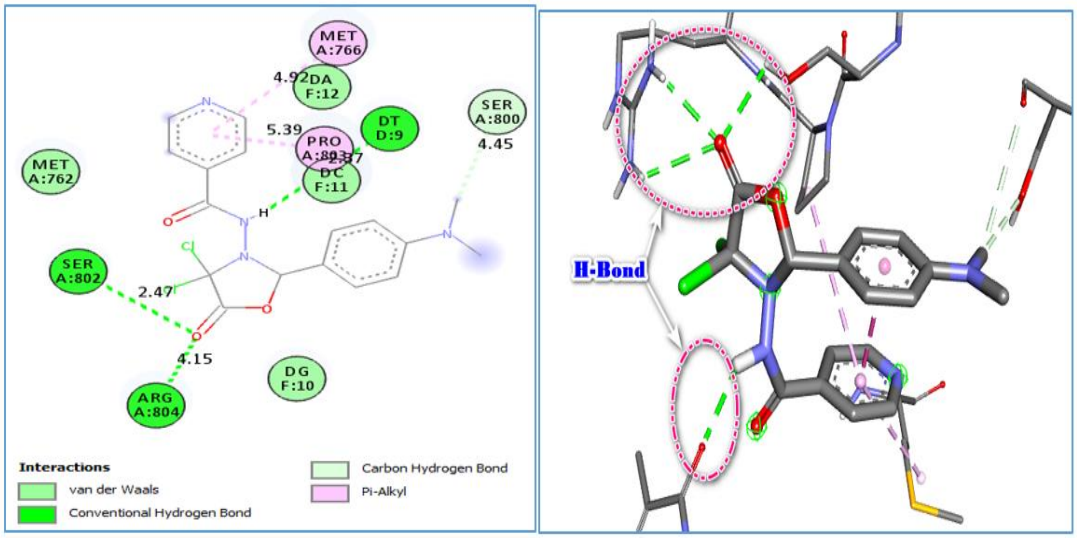

Fig. 24. Molecular docking between compound T9 with Human topoisomerase IIalpha enzyme(PDB:ID:5GWK) in 3D and 2D dimensions

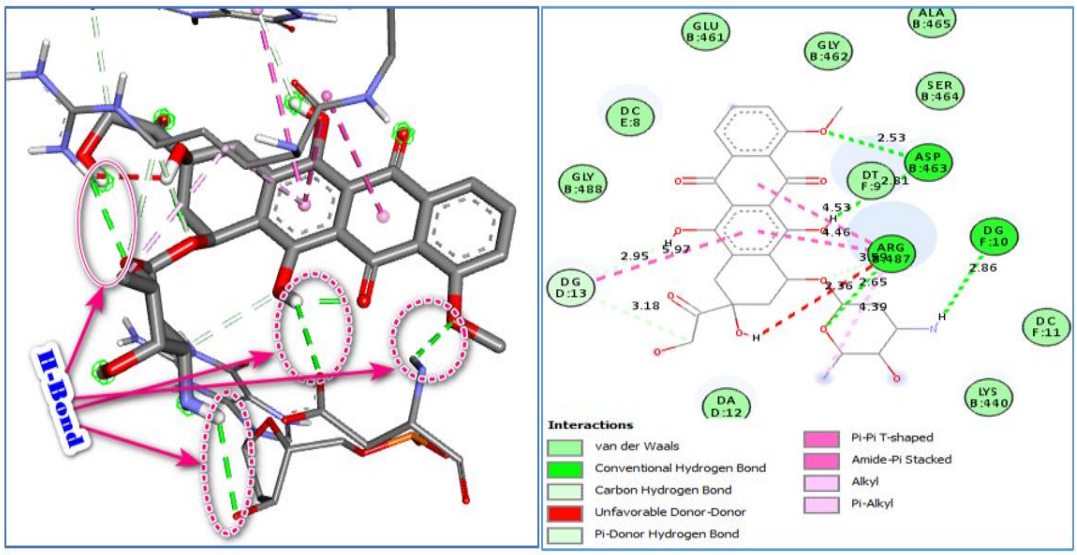

Fig. 25. Molecular docking between doxorubicin with binding site of Human topoisomerase IIalpha enzyme (PDB:ID:5GWK) in 3D and 2D dimensions

Anticancer Investigation of Derivatives T6–T10 of 4,4-Dichloro-1,3-Oxazolidine-5-One. The anticancer activities of the synthetic compounds were evaluated *in vitro* using the MTT assay on the breast cancer cell line MCF-7 (Fig. 26, Table 4). The results showed that compounds **T7** and **T9** exhibited promising anticancer activity, with **IC50** values of 32 µM and 29 µM, respectively, when compared to **doxorubicin**. These findings indicate that T7 and T9 demonstrate significant potential as anticancer agents against the MCF-7 breast cancer cell line (Fig. 27 and 28).

Table 4. Cytotoxicity of new oxazoline derivatives on MCF-7 cell line

Comp. No.	IC_{50} µg/mL
T6	129
T7	32
T8	163
T9	29
T10	142
doxorubicin	23

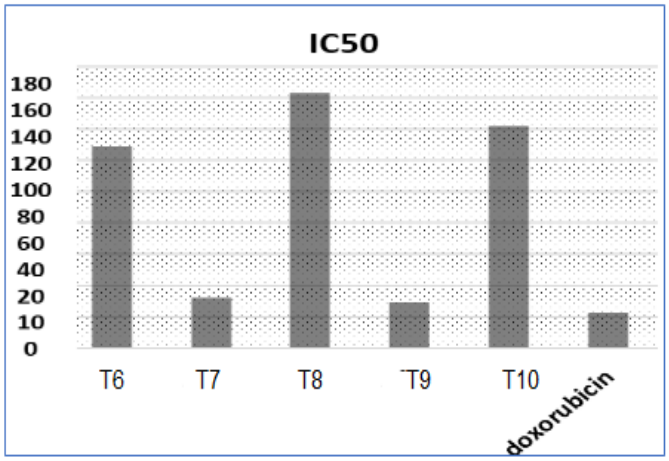

Fig. 26. Cytotoxicity of new oxazoline derivatives on MCF-7 cell line

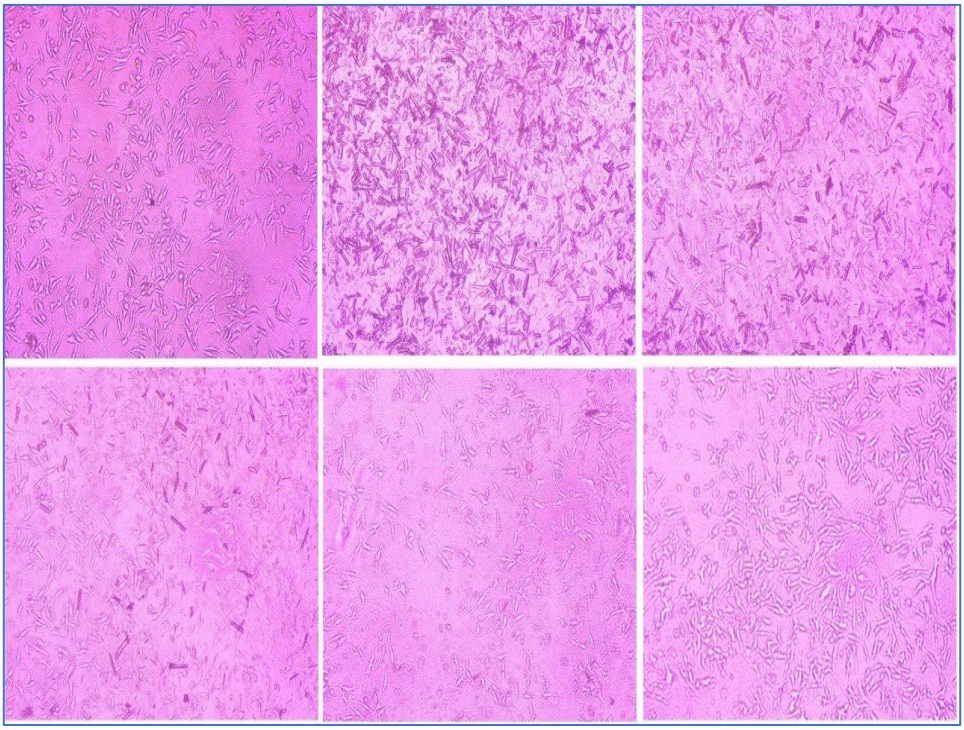

Fig. 27. Representative images of MCF-7 cells treated with varying concentrations of compound T7

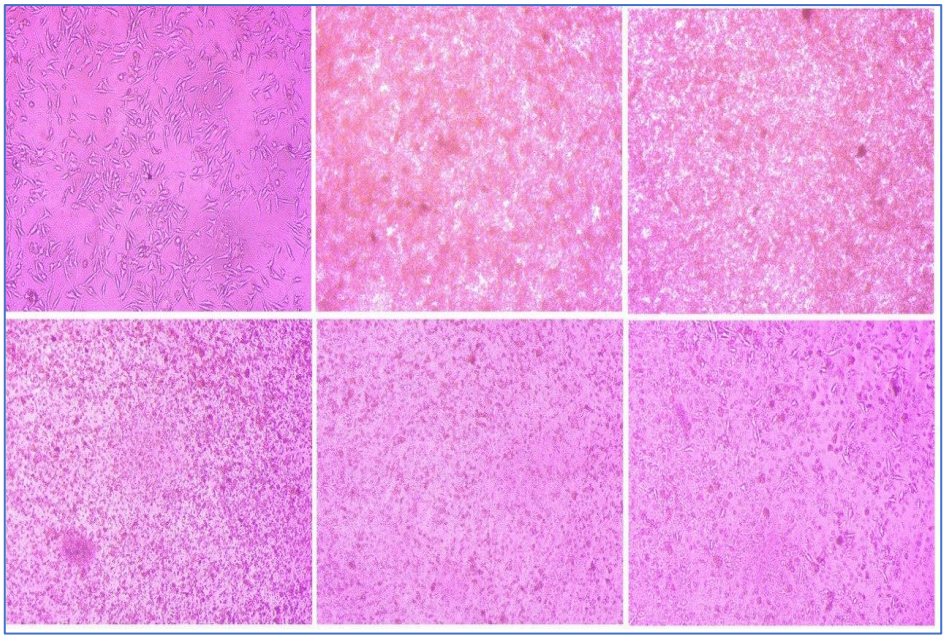

Fig. 27. Representative images of MCF-7 cells treated with varying concentrations of compound **T9**

Conclusions

The structures of the newly synthesized compounds were confirmed using FT-IR, ^{1}H-NMR, ^{13}C-NMR, and mass spectrometry. Compounds **T7 and T9 exhibited** significant anticancer activity against the MCF-7 breast cancer cell line. Molecular docking studies further supported these findings, showing favorable binding interactions with the human topoisomerase II alpha enzyme (PDB: ID: **5GWK**), characterized by low binding energy, a favorable RMSD value, and an ideal binding pattern.

Acknowledgments

We would like to express our gratitude to all individuals who have contributed significantly to the work presented in this publication, including those who provided technical support, writing assistance, editing, and general guidance.

References

1. Saini M.S., Kumar A., Dwivedi J., Singh R. A review: biological significances of heterocyclic compounds. *Int. J. Pharm. Sci. Res*, 2013, **Vol. 4(3)**, p. 66–77.
2. Al-Mulla A. A review: biological importance of heterocyclic compounds. *Der Pharma Chem.*, 2017, **Vol. 9(13)**, p. 141–147.
3. Volkova Y., Baranin S., Zavarzin I. A3 coupling reaction in the synthesis of heterocyclic compounds. *Adv. Synth. Catal.*, 2021, **Vol. 363(1)**, p. 40–61. DOI: 10.1002/adsc.202000866
4. Mermer A., Keles T., Sirin Y. Recent studies of nitrogen containing heterocyclic compounds as novel antiviral agents: A review. *Bioorg. Chem.*, 2021, **Vol. 114**, 105076. DOI: 10.1016/j.bioorg.2021.105076
5. Saurav P., Kuheli D., Sudip C. Fused ring heterocycle functionalized gold nanoparticles: synthesis and self-assembly. *Chemical Problems*, 2023, **Vol. 21(2)**, p. 188–196. DOI: 10.32737/2221-8688-2023-2-188-196
6. Zhang H.-Z., Zhao Z.-L., Zhou C.-H. Recent advance in oxazole-based medicinal chemistry. *Eur. J. Med. Chem.*, 2018, **Vol. 144**, p. 444–492. DOI: 10.1016/j.ejmech.2017.12.044
7. Lingala A.K., Murahari K.K., Desireddi J.R., Mothe T., Maiti B., Manchal R. Design, synthesis and biological evaluation of isoxazole bearing 1, 3-oxazole-1, 3, 4-oxadiazole derivatives as anticancer agents.

Chem. Data Collect., 2023, **Vol. 43**, 100959. DOI: 10.1016/j.cdc.2022.100959
8. Jin Z. Muscarine, imidazole, oxazole, and thiazole alkaloids. *Nat. Prod. Rep.*, 2011, **Vol. 28(6)**, p. 1143–1191. DOI: 10.1039/C7MD00067G
9. Thakur A., Verma M., Bharti R., Sharma R. Oxazole and isoxazole: From one-pot synthesis to medical applications. *Tetrahedron*, 2022, **Vol. 119**, 132813. DOI: 10.1016/j.tet.2022.132813
10. Abram J.A, Patel P. *Zolmitriptan*. 2020.
11. Alshehri S., Alqarni M., Namazi NI., Naguib I.A., Venkatesan K., Mosaad Y.O., Pishnamazi M., Alsubaiyel A.M., Abourehab M.A.S. Design of predictive model to optimize the solubility of Oxaprozin as nonsteroidal anti-inflammatory drug. *Sci. Rep.*, 2022, **Vol. 12(1)**, p. 13106. DOI: 10.1038/s41598-022-17350-5
12. Wang J., Zhang M ., Feng Y.-Q., Ma Ch.-Sh., Wang T.-D., Zhu Z.-M., Kario K. Is the newest angiotensin-receptor blocker azilsartan medoxomil more efficacious in lowering blood pressure than the older ones? A systematic review and network meta-analysis. *J. Clin. Hypertens.*, 2021, **Vol. 23(5)**, p. 901–914. DOI: 10.1111/jch.14227
13. Kakkar S., Narasimhan B. A comprehensive review on biological activities of oxazole derivatives. *BMC Chem.*, 2019, **Vol. 13(1)**, p. 1–24. DOI: 10.1186/s13065-019-0531-9
14. Gujjarappa R., Sravani S., Kabi A.K., Garg A., Vodnala N., Tyagi U., Kaldhi D., Singh V., Sreya Gupta S., Malakar Ch.C. *An overview on biological activities of oxazole, isoxazoles and 1, 2, 4-oxadiazoles derivatives.* In: Swain, B.P. (eds) Nanostructured Biomaterials. Materials Horizons: From Nature to Nanomaterials. Springer. Singapore. DOI: 10.1007/978-981-16-8399-2_10
15. Barreca M., Spanò V., Raimondi M.V., Tarantelli Ch., Spriano F., Bertoni F., Barraja P., Montalbano A. Recurrence of the oxazole motif in tubulin colchicine site inhibitors with anti-tumor activity. Eur. J. Med. Chem. Reports, 2021, Vol. 1, 100004. DOI: 10.1016/j.ejmcr.2021.100004
16. Hasanova S.S. Synthesis, physicochemical study and crystal structure of bis-(pnitrobenzoate)-di-(pyrazine) nickel (ii)-dihydrate. *Chemical Problems*, 2022, **Vol. 20(1)**, p. 95–101. DOI: 10.32737/2221-8688-2022-1-95-101
17. Foti C., Piperno A., Scala A., Giuffrè O. Oxazolidinone antibiotics: chemical, biological and analytical aspects. *Molecules*, 2021, **Vol. 26(14)**, p. 4280. DOI:10.3390/molecules26144280
18. Jiang J., Hou Y., Duan M., Wang B., Wu Y., Ding X., Zhao Y. Design, synthesis and antibacterial evaluation of novel oxazolidinone derivatives nitrogen-containing fused heterocyclic moiety. *Bioorg. Med. Chem. Lett.*, 2021, **Vol. 32**, 127660. DOI: 10.1016/j.bmcl.2020.127660
19. Gros C., Fahy J., Halby L., Dufau I., Erdmann A., Gregoire J.-M., Ausseil F., Vispé S., Arimondo P.B. DNA methylation inhibitors in cancer: recent and future approaches. *Biochimie*, 2012, **Vol. 94(11)**, p. 2280–2296. DOI: 10.1016/j.biochi.2012.07.025
20. Dong D., Xu Z., Zhong W., Peng S. Parallelization of Molecular Docking: A Review. *Curr. Top. Med. Chem.*, 2018, **Vol. 18(12)**, p. 1015–1028. DOI: 10.2174/1568026618666180821145215.
21. Kuntz I.D., Blaney J.M., Oatley S.J., Langridge R., Ferrin T.E. A geometric approach to macromolecule-ligand interactions. *J. Mol. Biol.*, 1982, **Vol. 161(2)**, p. 269–288. DOI: 10.1016/0022-2836(82)90153-X
22. Dias R., de Azevedo J., Walter F. Molecular docking algorithms. *Curr. Drug Targets*, 2008, **Vol. 9(12)**, p. 1040–1047. DOI: 10.2174/138945008786949432
23. Prieto-Martínez F.D., Arciniega M., Medina-Franco J.L. Molecular docking: current advances and challenges. *TIP. Rev. Espec. en ciencias químico-biológicas*, 2018, **Vol. 21**, DOI: 10.22201/fesz.23958723e.2018.0.143
24. Fan J., Fu A., Zhang L. Progress in molecular docking. *Quant. Biol.*, 2019, **Vol. 7**, p. 83–89. DOI: 10.1007/s40484-019-0172-y
25. Agarwal S., Mehrotra R. An overview of molecular docking. *JSM Chem*, 2016, **Vol. 4(2)**, p. 1024–1028.
26. Sulimov V.B., Kutov D.C., Sulimov A.V. Advances in Docking. *Curr. Med. Chem.*,

2019, **Vol. 26(42)**, p. 7555–7580. DOI: 10.2174/0929867325666180904115000.
27. Gaba M., Gaba P., Singh S., Gupta G.D. An overview on molecular docking. *Int J Drug Dev Res*, 2010, **Vol. 2(2)**, p. 219–231.
28. Saleh R.H., Rashid W.M., Dalaf A.H., Al-Badrany K.A., Mohammed O.A. Synthesis of some new thiazolidinone compounds derived from schiff bases compounds and evaluation of their laser and biological efficacy. *Ann Trop Public Heal.*, 2020, **Vol. 23(7)**, p. 1012–1031. DOI: 10.36295/ASRO.2020.23728
29. Zhao H.-R., Meng X.-W. (Z)-2-[(2, 4-Dimethylphenyl) imino]-1, 3-thiazinan-4-one. *Acta Crystallogr. Sect. E Struct. Reports Online*, 2011, **Vol. 67(1)**, p. o110–o110. DOI:10.1107/S1600536810051147
30. Dawood Z.A., Khalid F.D., Hameed A.S. Synthesis, radical scavenging activity, antibacterial activity and molecular docking of a new thiazolidine-4-one and 1, 3, 4 oxadiazole derivatives of tolfenamic acid. *Synthesis (Stuttg).*, 2022, **Vol. 45(02)**, p. 5017-5031.
31. Rane R.A., Sahu N.U., Shah C.P. Synthesis and antibiofilm activity of marine natural product-based 4-thiazolidinones derivatives. *Bioorg. Med. Chem. Lett.*, 2012, **Vol. 22(23)**, p. 7131–7134. DOI: 10.1016/j.bmcl.2012.09.073
32. Mahmood A.A.J., Bahnam S.P. Docking, synthesis and β-lactamase inhibitory activity evaluation for new amide compounds. *Chemical Problems*, 2024, **Vol. 22(2)**, p. 139–149. DOI: 10.32737/2221-8688-2024-2-139-14
33. Abdullah I.Q., Jasim Kh.A., Hamdoon A.M. Synthesis and Study of Some New Histidine Derivatives. 2014, **Vol. 10(2)**, p. 88-94.
34. Faihan A.S., Reza Behjatmanesh-Ardakani Thaaer Khalil, K. A. J., Synthesis, characterization and theoritical study of some pyrazine carbohydrazide derivatives. *International Journal of Biological and Chemical Sciences Part B*, 2024, **Vol. 6(1)**, DOI: 10.33545/26646765.2024.v6.i1b.117
35. AL-Bayati K.A. Synthesis and study of some new mannich bases derived from Isatin (1H-Indole-2, 3-Dione) with Substituted Sulfonamides and Their Antimicrobial Activity. *Tikrit J. Pure Sci.*, 2012, **Vol. 17(2)**, p. 40–45.
36. Jasim K.A., Aziz N.M., Ashfaq M., Behjatmanesh-Ardakani R., Faihan A.S., Tahir M.N., Al-Janabi A.S., Dege N., Gesquiere A.J. Docking, DFT, and structural study of N-((1,5-dimethyl-3-oxo-2-phenyl-2,3-dihydro-1H-pyrazol-4-yl)carbamothioyl)benzamide. *Struct Chem* 2024, **Vol. 35**, p. 1411–1425. DOI: 10.1007/s11224-024-02278-5
37. AL-Joubory I.K.J., Albayati T.F.K., Albayati K.A.J., Tareq S., Mahmood A.-J. Synthesis, Characterization and biological activity of some oxadiazoles derivatives and thiadiazoles derivatives. *Diyala Jr. Pure Sci*, 2013, **Vol. 9(3)**, p. 47–56.